Magnetization plateau in diamond chains with delocalized interstitial spins

M. S. S. Pereira, F. A. B. F. de Moura, and M. L. Lyra
Instituto de Física, Universidade Federal de Alagoas, 57072-970 Maceió, Alagoas, Brazil
(Received 26 September 2007; revised manuscript received 19 November 2007; published 2 January 2008)

Several low-dimensional magnetic compounds exhibit magnetization plateaus as a result of the interplay between frustration and quantum fluctuations. Here, we investigate the thermodynamic properties of diamond chains on which competing interactions emerge from the local quantum hopping of interstitial $S=1/2$ spins which are intercalated between nodal Ising spins. Using an exact diagonalization and the decoration-iteration transformation, we compute the temperature and external field dependences of the magnetization, specific heat, susceptibility, and the full ground state phase diagram. Magnetization plateaus of $1/3$ are observed and related to field-driven transitions among four possible ground states: saturated paramagnetic, unsaturated paramagnetic, ferrimagnetic, and nodal antiferromagnetic. There is a range of hopping amplitudes and exchange mismatches for which the $1/3$ magnetization plateau occurs between finite values of the external field. The specific heat and magnetic susceptibility also show signatures of the competition between the possible ground states.

DOI: 10.1103/PhysRevB.77.024402 PACS number(s): 75.10.Pq, 75.40.Cx, 75.50.Gg, 75.10.Jm

I. INTRODUCTION

The collective behavior of antiferromagnetically coupled spins in low-dimensional systems has been a subject of long-standing interest in condensed matter physics due to the wide variety of possible scenarios these systems can display.[1] One of the most remarkable features is that the ground state of a quantum antiferromagnetic chain does not exhibit a saturated antiferromagnetic order, in contrast with its classical counterpart. Further, the energy spectrum of quantum antiferromagnetic chains with half-integer spins is gapless. As a consequence, the system responds continuously to an external magnetic field up to a field value strong enough to promote a saturated magnetization. On the other hand, the spectrum of chains with integer spins exhibits a finite spin gap between the ground and excited states, known as the Haldane gap.[2,3] In the presence of an external field, the gap persists up to a critical field value. In this regime, the system does not respond to the external field. The magnetization curve displays a plateau of zero magnetization up to this critical field value, above which the gap is closed and the system starts to become magnetized until a second characteristic field value signaling complete polarization.

The phenomenon of magnetization plateau has attracted much attention during the past decade. The emergence of the magnetization plateau in trimerized $S=1/2$ spin chains was first numerically found by Hida[4] and first analytically explained by Okamoto.[5] It has been demonstrated that plateaus at finite magnetizations can emerge also in trimerized integer spin chains[6] as well as in low-dimensional systems with competing interactions[7–11] and itinerant electrons.[12] Such plateaus are present even in frustrated chains with half-integer spins on which the ground state can undergo a transition between a gapless state to a dimerized one upon increasing the external magnetic field.[13–16] Among the several models with frustrated magnetic interactions, the spin-$1/2$ quantum Heisenberg model in a chain with diamond topology has been used as a simple prototype model to study the interplay of frustration and quantum fluctuations[17–19] as well as the emergence of magnetization plateaus at finite magnetic fields.[20–22] This model presents a plateau at $1/3$ of the saturation magnetization, which occurs between two critical field values. In this regime, the ground state corresponds to a dimerized state separated from the excited states by a spin gap. At the upper critical field, the gap closes and the system restarts to respond to the external field. A second plateau at $2/3$ of the saturation magnetization develops in a region of the parameter space before reaching the fully saturated state.[22] The thermodynamic behavior usually shows signatures of the presence of the underlaying competing interactions such as double peak structures in the specific heat and susceptibility.[23] A $1/3$ magnetization plateau was experimentally observed in the diamond chain compound $Cu_3(CO_3)_2(OH)_2$, known as azurite.[24] The experimental observations, which included also two peak structures in the specific heat and magnetic susceptibility, were found to agree well with the theoretical analysis based on exact diagonalization and density matrix renormalization group techniques.

Recently, the occurrence of magnetization plateaus was reported in model systems incorporating Ising-like spins, including trimetrized,[25] tetramerized,[26] and diamond chains.[27–30] In these models, a decoration-iteration mapping associated with a transfer matrix technique allows for an exact analytical calculation of thermodynamical quantities. The main qualitative difference to the behavior of the fully quantum Heisenberg models is the fact that the zero-temperature magnetization plateaus are connected by discontinuous jumps, an aspect related to the localized nature of the magnetic excitations.[15,31] The access to the analytically exact solution for the thermodynamics of this class of models has allowed a close investigation of the interplay between geometric frustration, quantum fluctuations, and anisotropy effects for a wide range of values of the relevant physical parameters. In particular, an enhanced magnetocaloric effect has been reported when frustration comes into play.[29]

Frustration is usually introduced in spin models by considering competing two-spin interactions acting within unit cells having localized spins. However, the spin-spin interac-

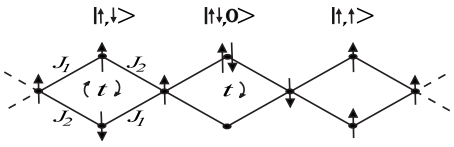

FIG. 1. Diagrammatic representation of the present diamond chain model. The corner (nodal) spins are Ising-like and localized. The exchange antiferromagnetic couplings are distinct along the nonparallel arms of the diamond units. Interstitial spins with antiparallel spins are allowed to hop within the inner sites of each diamond unit with hopping probability amplitude t. When they have parallel spins (as shown in the third cell), they are not allowed to hop due to Pauli's exclusion rule. The state vectors illustrate the notation used in the text.

tion is ultimately an effective coupling resulting from a process of electron exchange between neighboring sites. Very few rigorous analytical results are available for models that explicitly consider electron exchange processes. Here, we will introduce an exactly solvable model containing localized Ising-like spins and exchanging electrons in a diamond chain topology. We will show that the kinetic term produces antiferromagnetic correlations between the exchanging electrons leading to frustrated interactions. We will report the ground state phase diagram as a function of the external magnetic field and the mismatch of the Ising-like exchange couplings. The model exhibits ferrimagnetic and unsaturated paramagnetic phases with the occurrence of $1/3$ magnetization plateaus. We will compute the lower and upper fields delimiting the plateau regime as a function of the Ising-like couplings and the hopping amplitude of the delocalized electrons. Finally, we will compute the temperature dependence of the magnetization, specific heat, and magnetic susceptibilities, analyzing their main prominent features on the basis of the relevant energy scales involved in the model and the role played by thermal fluctuations.

II. MODEL: DIAMOND CHAIN WITH MOBILE INTERSTITIAL SPINS

In this work, we study a model with mixed localized Ising spins and mobile $S=1/2$ spins in the presence of an external magnetic field H. The sites belong to a diamond-like chain with localized Ising spins σ occupying the nodal sites. The interstitial sites of such diamond chain will be considered as having a single s orbital with one electron per site. The electrons of the interstitial sites are allowed to hop between the two interstitial sites forming a diamond loop, but are forbidden to hop to the nodal sites. The hopping process is restricted by Pauli's exclusion rule to occur only when the two mobile electrons have opposite spins. In such a case, a hopping amplitude t accounts for the kinetic energy associated with the electron mobility. The nodal electrons interact with the mobile electrons through exchange couplings J_1 and J_2 along each bond orientation, respectively, as illustrated in Fig. 1. In what follows, we will be particularly interested in the case of antiferromagnetic couplings.

The pair of mobile electrons within a diamond loop can assume six distinct configurations. Two of them correspond to parallel spins. In these configurations, the mobility is suppressed due to Pauli's principle and the electrons remain localized, one in each interstitial site. In these configurations, the interaction energy of the pair of interstitial electrons of the ith cell with the nodal Ising spins can be written as

$$\langle\uparrow,\uparrow|\mathcal{H}_i|\uparrow,\uparrow\rangle = -\langle\downarrow,\downarrow|\mathcal{H}_i|\downarrow,\downarrow\rangle = -(J_1+J_2)(\sigma_i+\sigma_{i+1}), \tag{1}$$

where σ_i and σ_{i+1} stand for the left and right nodal sites of cell i, respectively.

There are also four possible configurations with interstitial spins aligned antiparallel to each other. If both electrons occupy the same orbital, the exchange interaction with the nodal sites cancel out. Therefore,

$$\langle\uparrow\downarrow,0|\mathcal{H}_i|\uparrow\downarrow,0\rangle = \langle 0,\uparrow\downarrow|\mathcal{H}_i|0,\uparrow\downarrow\rangle = 0. \tag{2}$$

On the other hand, when antiparallel interstitial spins occupy distinct sites, there is a residual interaction energy due to the coupling mismatch given by

$$\langle\uparrow,\downarrow|\mathcal{H}_i|\uparrow,\downarrow\rangle = -\langle\downarrow,\uparrow|\mathcal{H}_i|\downarrow,\uparrow\rangle = -(J_1-J_2)(\sigma_i-\sigma_{i+1}). \tag{3}$$

Finally, the antiparalell states are mixed by the electron hopping between the interstitial sites. To take into account the hopping process, the interaction Hamiltonian must contain off-diagonal elements. Considering only single electron hopping, these non-null off-diagonal elements are

$$\langle\uparrow\downarrow,0|\mathcal{H}_i|\uparrow,\downarrow\rangle = \langle\uparrow\downarrow,0|\mathcal{H}_i|\downarrow,\uparrow\rangle = t, \tag{4}$$

$$\langle 0,\uparrow\downarrow|\mathcal{H}_i|\uparrow,\downarrow\rangle = \langle 0,\uparrow\downarrow|\mathcal{H}_i|\downarrow,\uparrow\rangle = t, \tag{5}$$

as well as their complex conjugates. In the presence of an external magnetic field H, the total Hamiltonian matrix can be written as

$$\mathcal{H} = \sum_i \mathcal{H}_i - \frac{1}{2}H(\sigma_i+\sigma_{i+1}) - H(S_{i,1}+S_{i,2}), \tag{6}$$

where $S_{i,1}=\pm 1$ and $S_{i,2}=\pm 1$ represent the spin orientation of each interstitial electron of the cell i. Due to the presence of off-diagonal terms, the stationary states of the cell Hamiltonian are composed of linear superpositions of the four states with antiparallel interstitial spins, in addition to the two parallel states. The possibility of electron hopping lowers one of the energy eigenvalues with respect to the exchange mismatch contribution, thus favoring the antiparallel alignment of interstitial spins in the limit of large hopping amplitudes.

III. GROUND STATE PHASE DIAGRAM

The above Hamiltonian model was exactly diagonalized, and the eigenstates and eigenenergies were obtained as a function of the external field H, coupling constants J_1 and J_2, and the hopping amplitude t. We identified that there are four possible ground states depending on the set of model parameters: a saturated paramagnetic state (SPA) with all spins

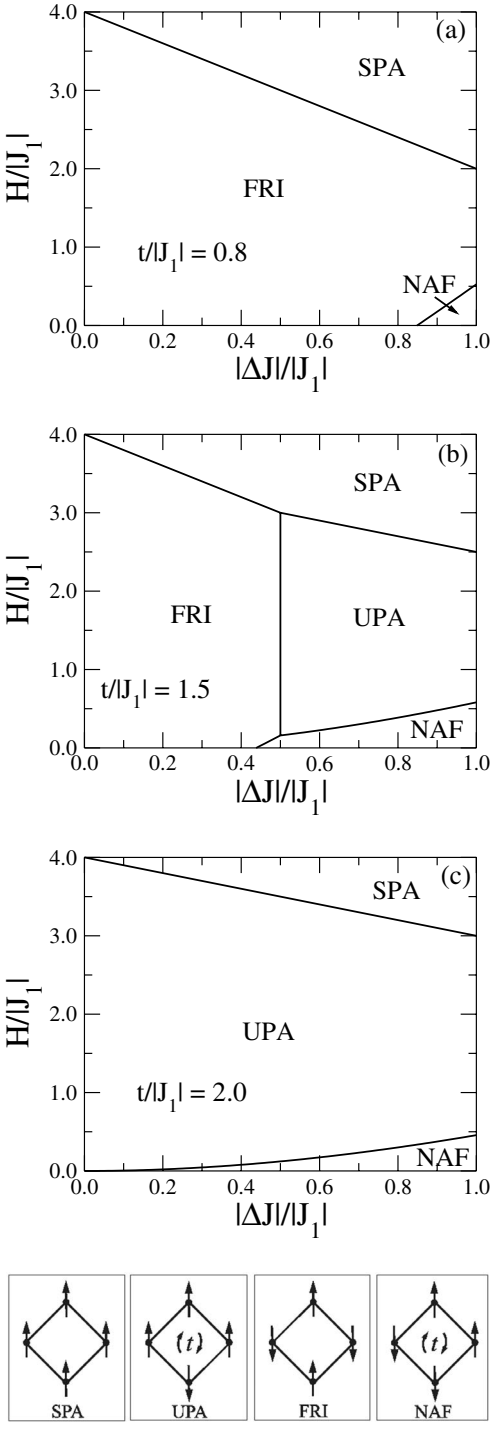

FIG. 2. Representative phase diagrams in the magnetic field H versus exchange mismatch ΔJ plane for distinct regimes of the hopping amplitude. (a) $t/|J_1| \leqslant 1$ for which the phase diagram exhibits three possible phases: SPA, FRI, and NAF. (b) $1 < t/|J_1| < 2$ for which the phase diagram also presents a region at which the UPA phase is stable. (c) $t/|J_1| \geqslant 2$ for which the only possible ground states are the SPA, UPA, and NAF. The NAF state has null magnetization per site, while the FRI and UPA have $1/3$ magnetization. The coexistence lines can be obtained by comparing the energies per unit cell of each phase as given by Eqs. (7)–(10). The ground state becomes degenerated with the first-order phase transitions occurring on these lines. (d) At the bottom, we sketch the unit cell configuration for the four possible ground states.

aligned in the field direction; an unsaturated paramagnetic state (UPA) with the nodal spins aligned in the field direction and the interstitial spins aligned antiparalell to each other; a ferrimagnetic state (FRI) with interstitial spins aligned parallel to the field and the nodal spins aligned in the opposite direction; and a nodal antiferromagnetic state (NAF) with the nodal spins obeying an antiferromagnetic sequence and the interstitial spins aligned antiparalell to each other. The energies per unit cell for these possible ground states are given by

$$E_{\mathrm{SPA}} = 4|J_1| - 2|\Delta J| - 3H, \tag{7}$$

$$E_{\mathrm{UPA}} = -2t - H, \tag{8}$$

$$E_{\mathrm{FRI}} = -4|J_1| + 2|\Delta J| - H, \tag{9}$$

$$E_{\mathrm{NAF}} = -2\sqrt{\Delta J^2 + t^2}, \tag{10}$$

where we have introduced the exchange mismatch $\Delta J = J_1 - J_2$ and assumed $|J_1| > |J_2|$ without any loss of generality.

In Fig. 2, we plot typical ground state phase diagrams in the magnetic field H versus exchange mismatch ΔJ plane. There are three distinct regimes depending on the ratio $t/|J_1|$. For $t/|J_1| \leqslant 1$ [Fig. 2(a)], the phase diagram exhibits three phases. For large magnetic fields, the SPA phase predominates. As the field is lowered, the system undergoes a transition to the FRI phase. The transition line corresponds to $E_{\mathrm{SPA}} = E_{\mathrm{FRI}}$. At very low fields, the NAF phase sets up in the regime of large exchange mismatches, with the transition line given by the condition $E_{\mathrm{FRI}} = E_{\mathrm{NAF}}$.

For $1 < t/|J_1| < 2$, the phase diagram presents all four possible ground states [Fig. 2(b)]. Below the SPA phase, the ferrimagnetic state is the most stable only in the regime of exchange mismatches $|\Delta J|/|J_1| < 2 - t/|J_1|$. Otherwise, the UPA phase takes place. At low fields, the NAF phase remains stable for large mismatches. At zero field, the NAF phase emerges for $|\Delta J|/|J_1| > 1 - (1/4)(t/|J_1|)^2$.

For $t/|J_1| \geqslant 2$, the ferrimagnetic state is no more stable for any exchange mismatch. The typical phase diagram is shown in Fig. 2(c). Notice that the zero-field ground state is always the nodal antiferromagnetic. As the field is increased, the system goes to the unsaturated paramagnetic phase and, finally, to the saturated paramagnetic phase. It is important to stress here that the antiferromagnetic phase has zero magnetization per site, while the intermediate ferrimagnetic and unsaturated paramagnetic phases have $1/3$ magnetization per site. This scenario favors the occurrence of $1/3$ magnetization plateaus, as we will discuss in the following section.

IV. EXACT DECORATION-ITERATION TRANSFORMATION

The thermodynamic properties of the present diamond chain model can be obtained through its exact mapping onto the one-dimensional Ising model with effective temperature dependent coupling J_{eff} and external field H_{eff}. Employing a decoration-iteration transformation,[32] the partition function for the present model can be written as

$$Z(T,J_1,J_2,t,H) = A^N Z_{\text{Ising}}(T,J_{\text{eff}},H_{\text{eff}}), \tag{11}$$

where Z_{Ising} is the partition function of the one-dimensional Ising model, N is the number of plaquettes of the diamond chain, and A, J_{eff}, and H_{eff} are derived after performing the partial trace over the possible states of the interstitial spins. The decoration-iteration mapping is based on the fact that the expression resulting from the partial trace can be put in an Ising-like form given by

$$\sum_k e^{-\beta\lambda_k(\sigma_i,\sigma_{i+1})} = A e^{\beta J_{\text{eff}}\sigma_i\sigma_{i+1}+(1/2)\beta H_{\text{eff}}(\sigma_i+\sigma_{i+1})}, \tag{12}$$

where $\beta=1/k_BT$, and $\lambda_k(\sigma_i,\sigma_{i+1})$ stands for the kth eigenvalue of the plaquette Hamiltonian with a fixed configuration of the nodal spins σ. The above transformation has been widely used to investigate the thermodynamic properties of decorated Ising models, such as the occurrence of reentrant transitions and compensation points[33,34] as well as the effects played by a transverse field, anisotropy, disorder, competing interactions, quantum fluctuations, and free surfaces.[25,26,29,35–40] In the present model, the partial trace extends over all six possible eigenvalues. The above relation holds for any configuration of the pair of nodal spins σ_i and σ_{i+1}. Therefore, the effective coupling, magnetic field, and normalization constant can be readily obtained. In particular, the effective field can be put in the form

$$e^{2\beta H_{\text{eff}}} = \frac{\sum_k e^{-\beta\lambda_k(1,1)}}{\sum_k e^{-\beta\lambda_k(-1,-1)}}. \tag{13}$$

Notice that in the absence of an external field acting on the plaquette spins, the effective field will be null due to the remaining up-down symmetry $[\lambda_k(1,1)=\lambda_k(-1,-1)]$. For the effective exchange coupling between the nodal spins, one obtains

$$e^{2\beta J_{\text{eff}}} = \frac{\left(\sum_k e^{-\beta\lambda_k(1,1)}\sum_k e^{-\beta\lambda_k(-1,-1)}\right)^{1/2}}{\sum_k e^{-\beta\lambda_k(1,-1)}}, \tag{14}$$

while the normalization constant can be written as

$$A^2 = \left(\sum_k e^{-\beta\lambda_k(1,1)}\sum_k e^{-\beta\lambda_k(-1,-1)}\right)^{1/2}\sum_k e^{-\beta\lambda_k(1,-1)}. \tag{15}$$

The eigenvalues of the Hamiltonian plaquette for each configuration of the nodal spins are summarized in Table I. The explicit expressions for the effective coupling and magnetic field are quite lengthy and do not bring any additional information to deserve being shown. From the above equations, and by exploiting the solution of the one-dimensional Ising model, the complete thermodynamical behavior of the present model can be analyzed.

V. 1/3 MAGNETIZATION PLATEAUS AND RESPONSE FUNCTIONS

In this section, we report on the behavior of some relevant thermodynamic quantities which are able to reveal the competition between the possible ground states of the present diamond chain model. To this end, we will consider periodic boundary conditions. The Helmholtz free energy can be obtained from $f(T,H)=\lim_{N\to\infty}-\frac{k_BT}{3N}\ln Z(T,H)$. The magnetization $m=-(\partial f/\partial H)_T$, the magnetic susceptibility $\chi=(\partial m/\partial H)_T$, the internal energy $u=-\frac{1}{3N}(\partial \ln Z/\partial\beta)_H$, and the specific heat $c=(\partial u/\partial T)_H$ follow straightforwardly. All quantities are computed per spin.

TABLE I. Eigenvalues of the plaquette Hamiltonian for different configurations of the pair of nodal spins. The first two eigenvalues correspond to the states where the interstitial spins are parallel. The eigenvalue λ_6 corresponds to the eigenstate for which the electron hopping between the interstitial sites promotes a lowering of the energy level.

	$\sigma_i=\sigma_{i+1}=1$	$\sigma_i=\sigma_{i+1}=-1$	$\sigma_i=-\sigma_{i+1}$
λ_1	$-2(J_1+J_2)-3H$	$2(J_1+J_2)-H$	$-2H$
λ_2	$2(J_1+J_2)+H$	$-2(J_1+J_2)+3H$	$2H$
λ_3	$-H$	H	0
λ_4	$-H$	H	0
λ_5	$2t-H$	$2t+H$	$2\sqrt{\Delta J^2+t^2}$
λ_6	$-2t-H$	$-2t+H$	$-2\sqrt{\Delta J^2+t^2}$

In Fig. 3, we plot the field dependence of the magnetization per site for distinct temperatures in two representative situations. In Fig. 3(a), the zero-field ground state corresponds to a ferrimagnetic phase for which the magnetization per site is 1/3 of the saturation magnetization. This state is equivalent to the ferrimagnetic state reported to appear in distorted diamond chains with antiferromagnetically coupled localized Heisenberg $S=1/2$ spins.[22] The zero-temperature curve exhibits a well defined 1/3 magnetization plateau up to the critical field, above which the saturated paramagnetic phase becomes the stable equilibrium state. The magnetization is discontinuous at the transition signaling the first-order zero-temperature phase transition. At finite temperatures, thermal fluctuations round off the discontinuity. However, the 1/3 magnetization plateau is still present in a wide range of magnetic field values at low temperatures. The magnetization curves for different temperatures cross roughly at a single point, which signals the critical field.

In Fig. 3(b), we show the magnetization curves for a set of parameters for which the zero-field ground state is the NAF phase. This state has zero magnetization per site. As the field strength is increased, the ground state exhibits a transition to the UPA phase, which has 1/3 magnetization per site. In this state, the nodal spins are aligned parallel to the external field, while the interstitial spins form dimers with zero spin. This state has a close analogy with the one leading to the magnetization plateau B discussed in Ref. 22. Due to the Ising nature of the nodal spins of the present model, the mechanism leading to the plateau A of Heisenberg distorted diamond chains cannot be realized. At larger magnetic fields, a second transition to the SPA phase sets up. The 1/3 magnetization plateau is restricted to a range of magnetic fields located between two finite values $H_{c,1}$ and $H_{c,2}$. The transitions at $H_{c,1}$ and $H_{c,2}$ are both discontinuous. Once again,

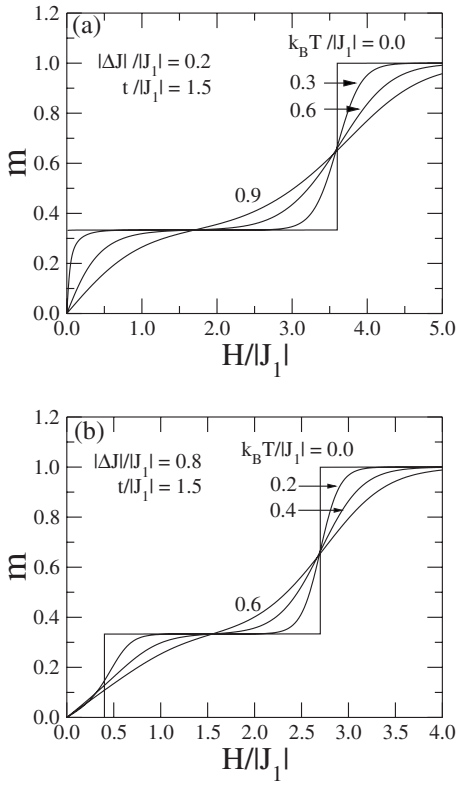

FIG. 3. Field dependence of the magnetization per spin for two representative cases. (a) FRI is the zero-field ground state. In this case, two distinct regimes are seen at zero temperature: a 1/3 magnetization plateau below a critical field and the saturation plateau. For finite temperatures, thermal fluctuations round off the magnetization jump. (b) NAF is the zero-field ground state. Here, three regimes are seen: a zero magnetization plateau at low fields, a 1/3 magnetization plateau at intermediate fields, and the saturation plateau. At finite temperatures, the curves cross roughly at a single point signaling the upper critical field. The low field crossing is somewhat spread.

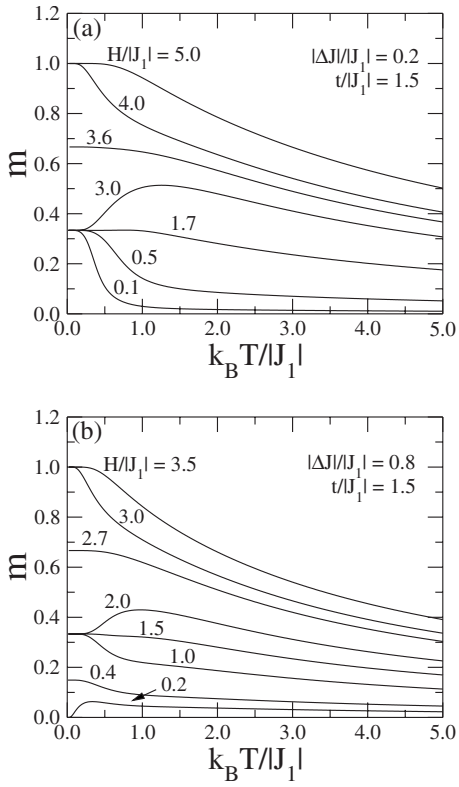

FIG. 4. Temperature dependence of the magnetization per site for two representative cases. (a) FRI is the zero-field ground state. In this case, two distinct regimes are seen, as in Fig. 3. At the critical field, the zero-temperature magnetization is 2/3 of the saturation value due to the degeneracy of the SPA and FRI states. (b) NAF is the zero-field ground state. At the lower and upper critical fields, the zero-temperature magnetization per site is $\sqrt{5}/15$ and 2/3, respectively. These values correspond, respectively, to the degeneracy between the NFA and UPA states, and between the UPA and SPA states.

thermal fluctuations smoothen the magnetization curves and just continuous crossovers are observed. The curves from different temperatures also cross roughly at a single point near the crossover from the 1/3 magnetization plateau to the saturation plateau. However, the crossing points near the crossover from zero magnetization to 1/3 magnetization are quite spread, which might make the identification of the critical field from finite temperature measurements difficult.

In Fig. 4, we show the temperature dependence of the magnetization per site for several field values. In Fig. 4(a), the Hamiltonian parameters were chosen in order to have a ferrimagnetic ground state at zero field. The results show clearly the two regimes corresponding to the ferrimagnetic ground state and the saturated paramagnetic ground state. Exactly at the critical field, the zero-temperature magnetization is 2/3 as the SPA and FRI states become degenerated. In Fig. 4(b), the parameter set was chosen to provide a NAF zero-field ground state. In this case, there are three distinct magnetic field regimes corresponding to zero, 1/3, and saturated zero-temperature magnetizations. At the lower critical field value, the zero-temperature magnetization is $\sqrt{5}/15$ due to the degeneracy of the NAF and UPA states. This value is in agreement with the magnetization per cell of antiferromagnetic Ising chains under the critical field. At this point, the ground state is actually macroscopically degenerate with all nodal spin configurations, except those which contain neighboring nodal spins pointing opposite to the field direction, having the same energy.[41,42] At the upper critical field value, a 2/3 zero-temperature magnetization reflects the degeneracy of the UPA and SPA states.

At zero magnetic field, the system presents two possible ground states depending on the exchange mismatch and hopping amplitude, namely, the FRI and the NAF states. The thermodynamic behavior of typical response functions can reveal the competition between these two states. In Fig. 5, we show the temperature dependence of the zero-field specific heat for $t/|J_1|=1.5$ and different values of the exchange mismatch ΔJ. For $|\Delta J|/|J_1|<1-(1/2)(T/|J_1|)^2$, the ground state is the FRI one. The NAF state becomes the ground state in the opposite regime. In Fig. 5(a), we show results for the set of exchange couplings which leads to a FRI ground state, while in Fig. 5(b), the ground state is the NAF state. Notice that the specific-heat curves develop a two-peak structure. The main peak is related to the development of dimerlike correlations between the nodal sites and the interstitial spins

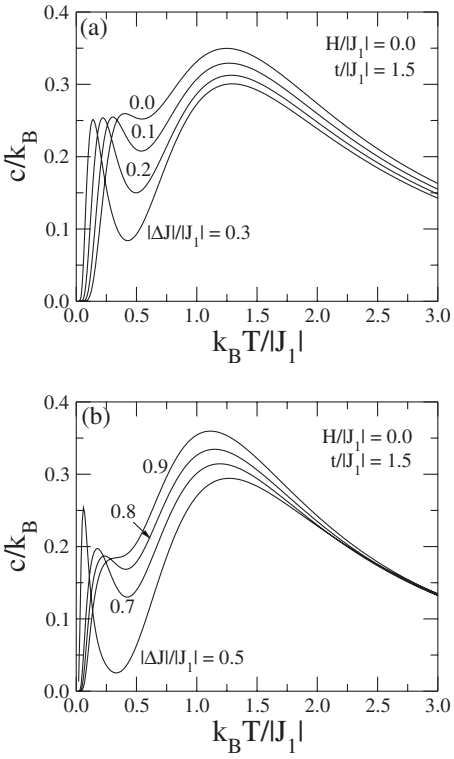

FIG. 5. Temperature dependence of the zero-field specific heat per site for two representative cases. (a) FRI is the ground state. (b) NAF is the zero-field ground state. A secondary peak appears in the vicinity of the critical mismatch separating these two possible ground states. Such peak appears at a temperature of the order of the difference between the energies of these competing ground states.

satisfying the largest exchange coupling J_1. Such correlation is common to both ground states. As the temperature is lowered, the dimers become correlated. However, this additional correlation is of distinct natures in the FRI and NAF phases. The typical temperature for the development of this additional correlation is of the order of the energy difference between these states $E_{\mathrm{FRI}}-E_{\mathrm{NAF}}$. At this temperature, the specific heat presents a secondary peak signaling the ultimate spin ordering. The second peak occurs at very low temperatures when the exchange mismatch is close to the critical value at which the FRI and NAF states are degenerate.

The zero-field magnetic susceptibility χ also presents a signature of the competition between the FRI and NAF ground states. In Fig. 6, we report the temperature dependence of $k_BT\chi$ for several exchange mismatches. For small mismatches, $k_BT\chi$ diverges as $T\rightarrow 0$, as expected for a ferrimagnetic phase. Above the critical mismatch, $k_BT\chi$ vanishes as $T\rightarrow 0$, signaling the nodal antiferromagnetic ground state. At the critical mismatch, the $T=0$ limit of $k_BT\chi$ reaches $1/3$ of the asymptotic high temperature value due to the degeneracy. The presence of competing ground states is reflected by the observed nonmonotonic temperature dependence of $k_BT\chi$.[23,43]

VI. SUMMARY AND CONCLUSIONS

In summary, we introduced an exactly solvable spin chain model containing localized and delocalized spins. The model

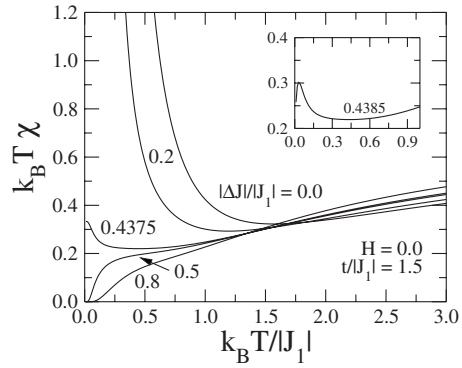

FIG. 6. Temperature dependence of the scaled zero-field susceptibility $k_BT\chi$ per site for distinct exchange mismatches. The divergence at low temperatures is typical of a ferrimagnetic ground state. It vanishes as $T\rightarrow 0$ in the regime of nodal antiferromagnetic ground state, while it goes to a constant value at the degenerating exchange mismatch. The nonmonotonic behavior is the main signature of the presence of competing ground states. The inset is an amplification of the nonmonotonic behavior slightly inside the NAF phase.

consists of a one-dimensional sequence of diamond-shaped units. The corner-sharing positions of the diamond units are occupied by localized Ising spins, while the two spins within the inner sites of each diamond unit are allowed to hop from one site to the other, although obeying Pauli's exclusion principle. These delocalized interstitial spins are coupled antiferromagnetically to the corner spins. The model considers the general case of anisotropic exchange couplings. We restricted our study to the case with no on-site Coulomb repulsion effects on the interstitial sites. While the inclusion of such term is straightforward, its main effect is to favor the localization of the interstitial spins.

In the absence of mobility of the internal spins within each diamond unit, the system has a single ground state in the absence of an external field. In this state, the internal spins are aligned antiparallel to the corner spins. This configuration represents a ferrimagnetic order whose magnetization per spin is $1/3$ of the saturation magnetization. In this case, the system presents no frustration. Whenever the interstitial spins are allowed to hop within the inner sites of each diamond unit with a probability amplitude t, there is a lowering of the local energy, thus favoring an antiferromagnetic correlation between the interstitial spins. This kinetically induced antiferromagnetic coupling, acting together with the exchange coupling to the corner spins, introduces frustration. As a result, a new ground state is possible, named a nodal antiferromagnetic state, where the corner spins follow an antiferromagnetic order and the interstitial spins are aligned antiparallel to each other. This state has null magnetization per site. At finite magnetic fields, the kinetic term also favors the emergence of an unsaturated paramagnetic phase with $1/3$ magnetization, in which the corner spins are aligned parallel to the external field while the interstitial spins are antiferromagnetically correlated. By performing an exact diagonalization of the plaquette Hamiltonian, we computed all energy eigenstates and reported a detailed phase diagram for different values of the magnetic field, exchange mismatch, and hopping amplitude.

Using the decoration-iteration mapping, we computed the exact partition function of the present model to obtain its thermodynamic behavior. In particular, we showed that a finite hopping amplitude favors the emergence of a 1/3 magnetization plateau within a range of finite magnetic field values. This feature reflects the competition between the possible ground states introduced by the kinetically induced frustration. At finite temperatures, the edges of the magnetization plateau are rounded off by thermal fluctuations, with the magnetization curves from distinct temperatures roughly crossing at a single point, signaling the change on the underlaying magnetic ordering. The temperature dependence of the magnetization for distinct field values clearly shows the regimes of zero, 1/3, and saturated magnetizations. At the magnetic field values corresponding to the edges of the 1/3 magnetization plateau, the magnetization curves present intermediate values as $T \to 0$ due to the degenerated nature of the ground state. The temperature dependences of the zero-field specific heat present a two-peak structure which reflects the competition between the two possible ground states. We also reported the zero-field magnetic susceptibility, which also exhibits a competing trend.

In conclusion, we have shown that 1/3 magnetization plateaus can emerge in a diamond chain model where frustration is induced by a hopping probability amplitude which takes into account a delocalized nature of the spins. By restricting the quantum hopping to occur within each diamond unit, the model could be exactly solved and its thermodynamic properties fully investigated as a function of the Hamiltonian parameters. Such kinetically induced frustration is expected to take place in more complex geometries. For an extension of the present model to include the quantum hopping of spins between neighboring unit cells, an exact solution is unlikely to be attainable for the thermodynamic quantities. Also, an extension to the case of localized Heisenberg nodal spins would not allow the use of the exact decoration-iteration mapping. In such cases, one shall rely on numerical results based on the study of finite systems, such as the exact diagonalization of the full Hamiltonian and density matrix renormalization group techniques. We hope the present work will stimulate further studies of the occurrence of magnetization plateaus in systems with localized Ising-like spins coupled to itinerant electrons.[44,45]

ACKNOWLEDGMENTS

We would like to thank partial financial support from CAPES, CNPq, CNPq-Rede Nanobioestruturas, and FINEP-CTInfra (Brazilian research agencies) as well as from FAPEAL (Alagoas State research agency).

[1] I. Bose, Curr. Sci. **88**, 62 (2005).
[2] F. D. M. Haldane, Phys. Lett. **93A**, 464 (1983).
[3] F. D. M. Haldane, Phys. Rev. Lett. **50**, 1153 (1983).
[4] K. Hida, J. Phys. Soc. Jpn. **63**, 2359 (1994).
[5] K. Okamoto, Solid State Commun. **98**, 245 (1996).
[6] M. Oshikawa, M. Yamanaka, and I. Affleck, Phys. Rev. Lett. **78**, 1984 (1997).
[7] K. Totsuka, Phys. Rev. B **57**, 3454 (1998).
[8] D. C. Cabra, A. Honecker, and P. Pujol, Phys. Rev. Lett. **79**, 5126 (1997).
[9] A. Honecker, F. Mila, and M. Troyer, Eur. Phys. J. B **15**, 227 (2000).
[10] A. Koga, K. Okunishi, and N. Kawakami, Phys. Rev. B **62**, 5558 (2000).
[11] J. Schulenburg and J. Richter, Phys. Rev. B **65**, 054420 (2002).
[12] R. R. Montenegro and M. D. Coutinho-Filho, Physica A **357**, 173 (2005).
[13] H. T. Diep, *Frustrated Spin Systems* (World Scientific, Singapore, 2005).
[14] F. Heidrich-Meisner, I. A. Sergienko, A. E. Feiguin, and E. R. Dagotto, Phys. Rev. B **75**, 064413 (2007).
[15] V. R. Chandra and N. Surendran, Phys. Rev. B **74**, 024421 (2006).
[16] K. Damle and T. Senthil, Phys. Rev. Lett. **97**, 067202 (2006).
[17] K. Takano, K. Kubo, and H. Sakamoto, J. Phys.: Condens. Matter **8**, 6405 (1996).
[18] K. Okamoto, T. Tonegawa, Y. Takahashi, and M. Kaburagi, J. Phys.: Condens. Matter **11**, 10485 (1999).
[19] H. T. Wang, J. Phys.: Condens. Matter **14**, 8033 (2002).
[20] T. Tonegawa, K. Okamoto, T. Hikihara, Y. Takahashi, and M. Kaburagi, J. Phys. Soc. Jpn. **69**, 332 (2000).
[21] T. Tonegawa, K. Okamoto, T. Hikihara, Y. Takahashi, and M. Kaburagi, J. Phys. Chem. Solids **62**, 125 (2001).
[22] K. Okamoto, T. Tonegawa, and M. Kaburagi, J. Phys.: Condens. Matter **15**, 5979 (2003).
[23] H. H. Fu, K. L. Yao, and Z. L. Liu, Phys. Rev. B **73**, 104454 (2006).
[24] H. Kikuchi, Y. Fujii, M. Chiba, S. Mitsudo, T. Idehara, T. Tonegawa, K. Okamoto, T. Sakai, T. Kuwai, and H. Ohta, Phys. Rev. Lett. **94**, 227201 (2005).
[25] V. R. Ohanyan and N. S. Ananikian, Phys. Lett. A **307**, 76 (2003).
[26] J. Strecka and M. Jascur, J. Phys.: Condens. Matter **15**, 4519 (2003).
[27] C. Vitoriano, F. B. de Brito, E. P. Raposo, and M. D. Coutinho-Filho, Mol. Cryst. Liq. Cryst. Sci. Technol., Sect. A **374**, 185 (2002).
[28] C. Vitoriano, M. D. Coutinho-Filho, and E. P. Raposo, J. Phys.: Condens. Matter **35**, 9049 (2002).
[29] L. Canová, J. Strecka, and M. Jascur, J. Phys.: Condens. Matter **18**, 4967 (2006).
[30] H. H. Fu, K. L. Yao, and Z. L. Liu, J. Magn. Magn. Mater. **305**, 253 (2006).
[31] J. Schulenburg, A. Honecker, J. Schnack, J. Richter, and H.-J. Schmidt, Phys. Rev. Lett. **88**, 167207 (2002).
[32] I. Syozi, in *Phase Transitions and Critical Phenomena*, edited by C. Domb and M. S. Green (Academic, New York, 1972), Vol. 1.
[33] S. Matasovska and M. Jascur, Physica A **383**, 339 (2007).
[34] J. Oitmaa J and W. H. Zheng, Physica A **328**, 185 (2003).
[35] M. L. Lyra and S. Coutinho, Physica A **155**, 232 (1989).

[36] M. L. Lyra and S. B. Cavalcanti, Phys. Rev. B **45**, 8021 (1992).
[37] J. Strecka and M. Jascur, J. Magn. Magn. Mater. **260**, 415 (2003).
[38] N. C. Eddeqaqi, M. Saber, A. El-Atri, and M. Kerouad, J. Phys.: Condens. Matter **11**, 5603 (1999).
[39] T. Kaneyoshi, Phys. Rev. B **55**, 12497 (1997).
[40] T. Kaneyoshi, S. Shin, and T. Maeno, Physica A **262**, 441 (1999).
[41] C. Domb, Adv. Phys. **9**, 149 (1960).
[42] A. A. Ovchinnikov, D. V. Dmitriev, V. Y. Krivnov, and V. O. Cheranovskii, Phys. Rev. B **68**, 214406 (2003).
[43] D. Shiomi, M. Nishizawa, K. Sato, T. Takui, K. Itoh, H. Sakurai, A. Izuoka, and T. Sugawara, J. Phys. Chem. B **101**, 3342 (1997).
[44] S. Ishiwata, M. Lee, Y. Onose, N. P. Ong, M. Takano, and I. Terasaki, J. Magn. Magn. Mater. **310**, 1989 (2007).
[45] S. Ishiwata, I. Terasaki, F. Ishii, N. Nagaosa, H. Mukuda, Y. Kitaoka, T. Saito, and M. Takano, Phys. Rev. Lett. **98**, 217201 (2007).